

Quantum theory of an electron waiting time clock

David Dasenbrook¹ and Christian Flindt²

¹Département de Physique Théorique, Université de Genève, 1211 Genève, Switzerland

²Department of Applied Physics, Aalto University, 00076 Aalto, Finland

(Dated: June 27, 2022)

The electron waiting time is the time that passes between two subsequent charge transfers in an electronic conductor. Recently, theories of electron waiting times have been devised for quantum transport in Coulomb-blockade structures and for mesoscopic conductors, however, so far a proper description of a detector has been missing. Here we develop a quantum theory of a waiting time clock capable of measuring the distribution of waiting times between electrons above the Fermi sea in a mesoscopic conductor. The detector consists of a mesoscopic capacitor coupled to a quantum two-level system whose coherent precession we monitor. Under ideal operating conditions our waiting time clock recovers the results of earlier theories without a detector. We investigate possible deviations due to an imperfect waiting time clock. As specific applications we consider a quantum point contact with a constant voltage and lorentzian voltage pulses applied to an electrode.

I. INTRODUCTION

Recent breakthrough experiments have paved the way for giga-hertz quantum electronics.¹ Single electrons can now be emitted into low-dimensional circuits using either driven mesoscopic capacitors² or by applying lorentzian voltage pulses to a contact.^{3,4} Along with these advances follows the need to characterize the accuracy of such dynamic single-electron sources. To this end one may investigate the electron waiting time.⁵ This is the time that passes between two subsequent charge transfers in an electronic conductor. For an ideal single-electron emitter, the waiting time between subsequent emissions should be determined by the period of the external drive.^{6–10} In reality, however, the waiting time fluctuates for instance due to the uncertainty in the emission time or because of cycle-missing events. These fluctuations can be characterized by the distribution of electron waiting times.

Theories of electron waiting times have been developed both for quantum transport in Coulomb-blockade structures^{5,6,11–16} and for mesoscopic conductors.^{7,9,17–19} Electron waiting times have also been investigated in relation to transient quantum transport^{20,21} and for superconductors.^{22–24} In some Coulomb-blockade structures, the tunneling of individual electrons can be monitored in real-time,^{25–30} and the electron waiting time is clearly defined as the time that passes between two subsequent detections of a tunneling event. By contrast, in mesoscopic conductors, where the electronic transport is phase-coherent, the concept of electron waiting times is more subtle. In particular, it is not immediately obvious what physical process constitutes a detection event. As such, a proper definition of the electron waiting time relies on a careful description of a specific detector. In the context of full counting statistics, a quantum theory of a detector was developed by Levitov, Lee, and Lesovik.³¹

Existing theories of electron waiting times in mesoscopic conductors consider the electrons above the Fermi sea.^{7–10,17–19} For a fully transmitting single-channel conductor with an applied voltage V , it has been pre-

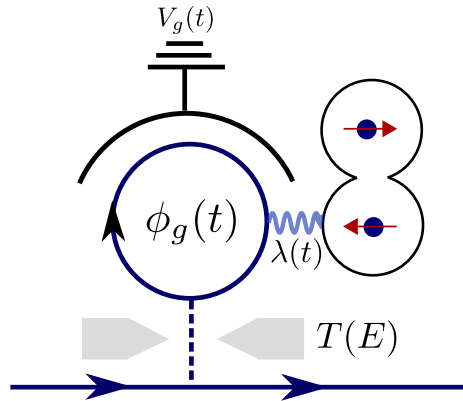


Figure 1. Electron waiting time clock. The clock consists of a mesoscopic capacitor coupled via a quantum point contact to a chiral edge state. Due to the energy-dependent transmission $T(E)$, only electrons above the Fermi level of the external reservoir can enter and leave the capacitor. Electrons inside the capacitor interact with a two-level system via the controllable coupling $\lambda(t)$. The top-gate potential $V_g(t)$ is used to empty the capacitor and leads to the time-dependent scattering phase $\phi_g(t)$. By monitoring the two-level system, the distribution of electron waiting times can be measured.

dicted that the distribution of electron waiting times should be given by a Wigner-Dyson distribution with the mean waiting time determined by the applied voltage as $\bar{\tau} = h/(eV)$.^{17,18} For typical voltages in the micro-volt regime, this mean waiting time is on the order of nanoseconds. This is a feasible time-scale from an experimental point of view. By contrast, if electrons in the Fermi sea are included, the mean waiting time would be given by the inverse Fermi energy, implying that a measurement of the electron waiting time essentially would be out of reach. Moreover, for dynamic single-electron sources, one is interested in the waiting time between the emission of electrons above the Fermi surface rather than in the intrinsic fluctuations in the Fermi sea.^{6–10} For these reasons, theories of waiting times between electrons above the Fermi sea are attractive.

It is well-known that measurements of zero-frequency quantities like the average current and the shot noise only concern the electrons above the Fermi level.^{32,33} On the other hand, measurements of the finite-frequency noise (and other short-time measurements) with standard current detectors are generally also sensitive to the underlying Fermi sea.³⁴ Bearing this in mind, it is clear that a theory of electron waiting times in mesoscopic conductors should include a description of a detector. This is the central goal of this paper. Specifically, we devise a quantum theory of a waiting time clock that is capable of measuring the distribution of waiting times between electrons above the Fermi sea in a mesoscopic conductor. When operated under ideal conditions, our waiting time clock recovers the results of earlier theories without a detector. Within our theoretical description, we can also investigate possible deviations due to imperfect operating conditions.

The rest of the paper is organized as follows. In Sec. II we discuss the scattering theory of full counting statistics (FCS) in mesoscopic conductors with a specific emphasis on the detector. In Sec. III we introduce the basic concepts of waiting time distributions (WTDs), including the idle time probability which will be important further on. In Sec. IV we describe our electron waiting time clock and its building blocks as indicated in Fig. 1. In Sec. V we illustrate the use of the waiting time clock with two specific applications. A possible implementation of the measurement scheme is described in Sec. VI. Finally, in Sec. VII, we present our conclusions and give an outlook on future work.

II. TIME-RESOLVED COUNTING STATISTICS

We start by recapitulating the scattering theory of time-dependent FCS with a special emphasis on the detector. An absorptive electron detector has been investigated theoretically in an early work.³⁵ As an alternative, Levitov, Lee, and Lesovik later on considered a detector which conserves the number of electrons.³¹ In this approach, the detector consists of a quantum two-level system, such as a spin-1/2 particle, which rotates coherently in the magnetic field induced by the electrical current in the conductor. The moment generating function of the FCS can then be measured directly as a function of the coupling strength between the spin and the conductor.

To see this, we consider the combined system, including the detector, described by the Hamiltonian

$$\hat{H}(t) = \hat{H}_{\text{el}}(t) + \hat{H}_{\text{int}}(t) = \hat{H}_{\text{el}}(t) - \lambda(t) \frac{\hbar}{2e} \hat{\sigma}_z \hat{I}. \quad (1)$$

The Hamiltonian of the conductor is denoted as $\hat{H}_{\text{el}}(t)$, $\hat{\sigma}_z$ is the Pauli matrix for the z -component of the spin, and \hat{I} is the operator for the electrical current through a given cross-section of the conductor. The particular form of the coupling between the spin and the conductor makes the spin rotate in the x - y plane of the Bloch

sphere due to the magnetic field induced by the electrical current. The coupling strength $\lambda(t)$ is assumed to be controllable and generally time-dependent. We evolve the combined system from $t = -\infty$ to $t = \infty$ and describe the finite duration of a measurement by having a coupling which is only non-zero during the measurement. (In a different approach,^{36,37} one detects the total charge in one of the leads at the beginning and at the end of the measurement and then defines the number of transferred charges as the difference between the two measurement outcomes.) After the complete time evolution, the electronic conductor is integrated out and the density matrix of the spin is obtained.

By evaluating the off-diagonal element of this reduced density matrix, one arrives at the function^{38–40}

$$\chi(\lambda) = \left\langle T \left\{ e^{i \int_{-\infty}^{\infty} dt \hat{H}_{-\lambda}(t) / \hbar} \right\} \tilde{T} \left\{ e^{i \int_{-\infty}^{\infty} dt \hat{H}_{\lambda}(t) / \hbar} \right\} \right\rangle, \quad (2)$$

where T and \tilde{T} denote time and anti-time ordering, respectively. The Hamiltonian $\hat{H}_{\lambda}(t)$ is obtained from Eq. (1) by replacing $\hat{\sigma}_z$ by unity so that it only acts on the electronic degrees of freedom. The electronic conductor consists of a central scatterer connected to electronic leads and is described by $\hat{H}_{\text{el}}(t)$. The electrons are non-interacting so that a scattering problem can be formulated in terms of a scattering matrix that we denote by \mathcal{S} . To include the coupling to the spin, we solve the scattering problem of the electrons interacting with the spin via the time-dependent coupling $\lambda(t)$ and denote the resulting scattering matrix by U_{λ} . Since both $\lambda(t)$ and $\hat{H}_{\text{el}}(t)$ can be time-dependent, neither U_{λ} nor \mathcal{S} are necessarily diagonal in the energy representation. The combined scattering matrix is denoted as \mathcal{S}_{λ} and will be specified in more detail in the following sections.

Equation (2) can be evaluated by means of the Keldysh technique.⁴¹ Specifically, it can be written as

$$\chi(\lambda) = \det \left(1 - n_F \left[1 - \mathcal{S}_{-\lambda}^{\dagger} \mathcal{S}_{\lambda} \right] \right), \quad (3)$$

which is known as the Levitov-Lesovik determinant formula. Here, n_F is the occupation matrix of the leads and the involved matrices have indices both in the channel and energy spaces.

For the special case of a single-channel chiral system, e. g. a quantum Hall edge state, there is no channel index. However, due to the general time-dependence of the problem, \mathcal{S}_{λ} is not diagonal in the energy representation. At zero temperature, n_F is just a projector onto the filled states in the lead from which electrons enter the conductor. We can then write Eq. (3) as

$$\chi(\lambda) = \det \left(\mathcal{S}_{-\lambda}^{\dagger} \mathcal{S}_{\lambda} \right), \quad (4)$$

where the matrix elements of $\mathcal{S}_{-\lambda}^{\dagger} \mathcal{S}_{\lambda}$ have been restricted to the initially filled states.

We now specify the interaction between the electrons and the spin. Due to the spin, electrons pick up the

additional scattering phase $\exp(i\lambda(t)/2)$. The scattering matrix U_λ therefore has the matrix elements

$$[U_\lambda]_{t,t'} = e^{i\lambda(t)/2} \delta(t - t') \quad (5)$$

in the time representation. We take an abrupt switching,

$$\lambda(t) = \lambda \Theta(t - t_0) \Theta(\tau - t + t_0), \quad (6)$$

where $\Theta(t)$ is the Heaviside step function, t_0 is the starting point of the measurement, τ is the duration, and λ is the coupling strength. In the energy representation, the matrix elements of U_λ then become

$$[U_\lambda]_{E,E'} = \delta(E - E') + K_\tau^\lambda(E - E'), \quad (7)$$

having defined

$$K_\tau^\lambda(E) = \left(e^{i\lambda/2} - 1 \right) K_\tau(E) \quad (8)$$

in terms of the sine kernel^{7,17,18}

$$K_\tau(E) = \frac{2}{E} e^{-i\frac{E(\tau+2t_0)}{2\hbar}} \sin\left(\frac{E\tau}{2\hbar}\right). \quad (9)$$

If the reservoirs are not initially in a superposition of different charge states, Eq. (3) can be interpreted as the moment generating function of the FCS.⁴² Specifically, from the inverse Fourier transformation

$$P(n) = \frac{1}{2\pi} \int_0^{2\pi} \chi(\lambda) e^{in\lambda} d\lambda, \quad (10)$$

we obtain the probability $P(n)$ that n charges have passed through the conductor while the detector was on. We note that backaction effects due to the measurement device are fully included in this formalism.

It is instructive to consider the limit of long measurement times. In this case, we can take $\lambda(t) \equiv \lambda$ to be constant in Eq. (6), such that U_λ becomes diagonal in the energy representation. If, furthermore, the Hamiltonian $\hat{H}_{\text{el}}(t) = \hat{H}_{\text{el}}$ is not time-dependent, the determinant over energies in Eq. (3) reduces to a product,

$$\chi(\lambda) = \prod_{E>0} \det \left(1 - [n_F]_{E,E} \left\{ 1 - [S_{-\lambda}^\dagger S_\lambda]_{E,E} \right\} \right), \quad (11)$$

where the determinant is now taken only over the channel indices of the matrices. For a single-channel two-terminal conductor with the energy-dependent transmission probability $T(E)$, contributions from left and right moving electrons below the Fermi level cancel each other at zero temperature and only electrons above the Fermi level need to be included,

$$\chi(\lambda) = \prod_{E_F > E > E_F + eV} [(e^{i\lambda} - 1)T(E) + 1]. \quad (12)$$

This type of FCS is known as generalized binomial statistics.⁴³⁻⁴⁵ The result shows us that observables measured over a long time, for instance the mean current or any zero-frequency current correlator, are only affected by the electrons in the voltage window $[E_F, E_F + eV]$ above the Fermi level. In the following we will see that finite-time measurements are more involved as they may also be influenced by electrons below the Fermi level.

III. WAITING TIME DISTRIBUTIONS

Building on the previous section, we are now ready to develop a quantum theory of an electron waiting time clock. We begin by establishing the general framework of WTDs before moving on to a detailed description of our detector.

In many physical systems, WTDs are used to characterize the random time that passes between two clicks of a detector. For example, in quantum optics, single-photon detectors can detect individual photons emitted from a light source.^{46,47} Also in Coulomb-blockade quantum dots, a nearby conductor can be used to monitor the charge state of the quantum dots and thereby detect the tunneling of individual charges in real-time.²⁵⁻³⁰ By contrast, in mesoscopic conductors, the detection of individual electrons is still challenging. Therefore, a careful analysis of the detection process is required.

Given a series of detection events, the waiting time is the time that elapses between two successive detections. The distribution of waiting times is denoted as $\mathcal{W}(\tau)$. For a stationary process, it can be related to the idle time probability $\Pi(\tau)$ as

$$\mathcal{W}(\tau) = \langle \tau \rangle \partial_\tau^2 \Pi(\tau), \quad (13)$$

where $\langle \tau \rangle$ is the mean waiting time.^{17,18} The idle time probability is the probability that no detections occur during a time interval of length τ , $[t_0, t_0 + \tau]$. For stationary processes, the idle time probability is independent of t_0 due to the translational invariance in time.^{17,18} By contrast, for periodically driven systems, it is a two-time quantity $\Pi(t_0, \tau)$ which explicitly depends on t_0 .^{7,9,10} The idle time probability entering Eq. (13) is then obtained as an average over the period of the driving \mathcal{T} ,^{7,9,10}

$$\Pi(\tau) = \frac{1}{\mathcal{T}} \int_0^{\mathcal{T}} \Pi(t_0, \tau) dt_0. \quad (14)$$

The idle time probability can also be expressed in terms of the time-dependent FCS as

$$\Pi(\tau) = P(n = 0, \tau) \quad (15)$$

which is the $n = 0$ component of the probability $P(n, \tau)$ to observe n detections during a time interval of length τ . Alternatively, the idle time probability can be expressed in terms of the moment generating function of the FCS

$$\chi(\lambda, \tau) = \sum_{n=0}^{\infty} P(n, \tau) e^{in\lambda}. \quad (16)$$

Specifically, we get $P(n = 0, \tau)$ by an inverse Fourier transformation as

$$P(n = 0, \tau) = \frac{1}{2\pi} \int_0^{2\pi} \chi(\lambda, \tau) d\lambda, \quad (17)$$

or, since the number of detector clicks is non-negative, by formally taking the limit $\lambda \rightarrow i\infty$,

$$P(n = 0, \tau) = \chi(\lambda \rightarrow i\infty, \tau). \quad (18)$$

Experimentally, one may measure the moment generating function $\chi(\lambda, \tau)$ for different values of the coupling strength λ and from those measurements evaluate the idle time probability using the Fourier transformation in Eq. (17). On the theory side, it will be useful rather to take the limit $\lambda \rightarrow i\infty$ according to Eq. (18).

The considerations above rely on a detector that produces a series of clicks. Since single-electron detection remains challenging in mesoscopic conductors, we proceed here along a different route and instead develop a detector that can measure the idle time probability of electrons above the Fermi sea in a mesoscopic conductor. As we will see, this leads to a well-defined distribution of waiting times between subsequent electron transfers.

IV. ELECTRON WAITING TIME CLOCK

The electron waiting time clock is depicted in Fig. 1. It consists of a mesoscopic capacitor^{48,49} coupled to a two-level quantum system, such as a spin-1/2 particle, in a similar spirit to the proposal to measure FCS by Levitov, Lee, and Lesovik.³¹ The coupling $\lambda(t)$ between the spin and the capacitor is controllable and time-dependent. We assume that the capacitor is initially depleted of electrons. As we will see, this setup makes it possible to measure the idle time probability and thus the WTD of electrons above the Fermi level in the incoming channel.

We start by constructing the scattering matrix of the electron waiting time clock. The capacitor is implemented with chiral edge states in the quantum Hall regime.² Incoming electrons in the edge state on the left may be transmitted into the capacitor via a QPC and make one or several round trips inside the capacitor before leaving via the outgoing edge state to the right. While being inside the capacitor, the electrons interact with the spin that we monitor. Importantly, as we discuss below, we use a QPC with a cut-off in the transmission close to the Fermi level.

The scattering matrix of the waiting time clock is obtained by summing up the amplitudes of all possible scattering processes. Formally, we can express it as

$$\mathcal{S}_\lambda = \mathcal{P}_R - \mathcal{P}_T \left[\mathcal{S}_\lambda^{(l)} \sum_{n=0}^{\infty} \left(\mathcal{P}_R \mathcal{S}_\lambda^{(l)} \right)^n \right] \mathcal{P}_T, \quad (19)$$

where the first term describes processes where electrons are reflected on the QPC and never enter the capacitor. The second term describes processes where electrons enter the capacitor and complete $n+1$ round trips (or loops) inside the capacitor before leaving via the outgoing edge state. We now specify each matrix in this expression.

We consider a QPC with an energy-dependent transmission $T(E)$. In a strong magnetic field, the transmission takes the form⁵⁰

$$T(E) = \frac{1}{e^{\mathcal{B}(E_F - E)} + 1}, \quad (20)$$

where the parameter \mathcal{B} can be controlled by the magnetic field. The QPC is tuned such that the transmission is cut off at the Fermi energy E_F . With this transmission profile, only electrons above the Fermi level are allowed to enter and leave the capacitor. The corresponding transmission and reflection matrices in Eq. (19) read

$$\begin{aligned} [\mathcal{P}_T]_{E,E'} &= \sqrt{T(E)} \delta(E - E'), \\ [\mathcal{P}_R]_{E,E'} &= \sqrt{1 - T(E)} \delta(E - E'). \end{aligned} \quad (21)$$

Next, we define the scattering matrix $\mathcal{S}_\lambda^{(l)}$ describing one round trip inside the capacitor. An electron inside the capacitor can make one or several round trips. For each completed loop, it picks up the scattering phase

$$[\mathcal{S}_\lambda^{(l)}]_{t,t'} = e^{i(\phi_g(t) + \lambda(t)/2)} \delta(t - t' - \tau_0), \quad (22)$$

where $\tau_0 = \ell/v_F$ is the time it takes to complete one loop with ℓ being the circumference of the capacitor and v_F the Fermi velocity. The specific times when the electron enters and leaves the capacitor are denoted as t' and t , respectively. The phase $\phi_g(t)$ picked up during one loop due to the time-dependent gate-voltage $V_g(t)$ reads

$$\phi_g(t) = \frac{e}{\hbar} \int_{t-\tau_0}^t V_g(t') dt'. \quad (23)$$

As we will see below, it is convenient to apply a linearly rising gate voltage of the form

$$V_g(t) = \delta V_g (t/\tau_0 + 1/2), \quad (24)$$

where δV_g is the increase of the voltage during one loop. In this case, the phase takes the simple form

$$\phi_g(t) = \frac{e\delta V_g}{\hbar} t. \quad (25)$$

Finally, the coupling to the spin $\lambda(t)$ is given by Eq. (6).

In the energy representation, the scattering matrix is non-diagonal with matrix elements reading

$$\begin{aligned} [\mathcal{S}_\lambda^{(l)}]_{E,E'} &= [\delta(E - E' - e\delta V_g) + K_\tau^\lambda (E - E' - e\delta V_g)] \\ &\quad \times e^{i(E' + e\delta V_g)\tau_0/\hbar}. \end{aligned} \quad (26)$$

This is the probability amplitude for a particle with incoming energy E' to change its energy to E due to the interaction with the spin and the time-dependent voltage.

Having specified the various scattering matrices, we can construct the scattering matrix of the electron waiting time clock according to Eq. (19). Moreover, if an additional scatterer (whose WTD we wish to measure) with scattering matrix \mathcal{S}_{sys} is placed before the waiting time clock, the full scattering matrix becomes

$$\mathcal{S}_\lambda^{(\text{tot})} = \mathcal{S}_\lambda \mathcal{S}_{\text{sys}}. \quad (27)$$

In the following section, where we apply our method, we specify \mathcal{S}_{sys} for two particular scatterers.

We start by considering the limit of a sharp cut-off in Eq. (20), where $\mathcal{B} \gg 1/E$ for all relevant energies. In this case, only electrons above the Fermi level are allowed to enter and leave the capacitor. Mathematically, the transmission and reflection matrices in Eq. (21) become projectors onto energies above and below the Fermi level which we denote as P_T and P_R , respectively. We can then evaluate the geometric series in Eq. (19) and write the scattering matrix as

$$\begin{aligned} \mathcal{S}_\lambda &= P_R - P_T \mathcal{S}_\lambda^{(l)} P_T \\ &\quad - P_T \mathcal{S}_\lambda^{(l)} P_R (1 - P_R \mathcal{S}_\lambda^{(l)} P_R)^{-1} P_R \mathcal{S}_\lambda^{(l)} P_T, \end{aligned} \quad (28)$$

having used properties of the projectors. This expression has a clear physical interpretation as we now discuss.

The first term corresponds to electrons below the Fermi level which are reflected on the QPC and never enter the capacitor. The second term describes electrons above the Fermi level that enter the capacitor, interact with the spin and the time-dependent voltage, but stay above the Fermi level, so that they leave the capacitor after having completed just one loop. The third term describes electrons that complete more than one loop. Read from right to left, this term corresponds to processes, where an electron above the Fermi level enters the capacitor and is scattered below the Fermi level during the first loop as described by the matrix product $P_R \mathcal{S}_\lambda^{(l)} P_T$. The electron then completes a number of loops (possibly none) below the Fermi level. This is described by the matrix inversion $(1 - P_R \mathcal{S}_\lambda^{(l)} P_R)^{-1}$, which can be re-expanded as a geometric series. Finally, in one last loop, the electron is scattered back above the Fermi level and leaves the capacitor as described by the matrix product $P_T \mathcal{S}_\lambda^{(l)} P_R$.

Ideally, the electron waiting time clock would be described by only the two first terms of the scattering matrix in Eq. (28). Electrons above the Fermi level then interact only once with the spin, while electrons below the Fermi level are filtered out. However, due to the time-dependence of the measurement procedure, the third term is generally present. To suppress processes where electrons complete several loops and interact with the spin more than once, we apply the top-gate voltage. With a sufficiently large voltage increase, we can ensure that essentially all electrons end up with an energy above the Fermi level after having completed the first loop, even if they may have lost energy by interacting with the spin. They will then leave the capacitor via the QPC after having interacted with the spin only once.

In this case, we can write the scattering matrix as

$$\mathcal{S}_\lambda = P_R - P_T \mathcal{S}_\lambda^{(l)} P_T, \quad (29)$$

without processes involving several loops. In the following section, we discuss the values of δV_g in Eq. (24) needed for this to be a good approximation. To evaluate the determinant formula in Eq. (3), we first note that

$$(\mathcal{S}_{-\lambda}^{(\text{tot})})^\dagger \mathcal{S}_\lambda^{(\text{tot})} = \mathcal{S}_{\text{sys}}^\dagger \left(P_R + P_T (\mathcal{S}_{-\lambda}^{(l)})^\dagger \mathcal{S}_\lambda^{(l)} P_T \right) \mathcal{S}_{\text{sys}}, \quad (30)$$

having used $[P_T, \mathcal{S}_\lambda^{(l)}] = 0$, since electrons that enter the capacitor remain above the Fermi level. This holds for large values of δV_g . A simple calculation now shows that

$$(\mathcal{S}_{-\lambda}^{(l)})^\dagger \mathcal{S}_\lambda^{(l)} = 1 + (e^{i\lambda} - 1) \mathcal{K}_\tau, \quad (31)$$

with the matrix elements

$$[\mathcal{K}_\tau]_{E,E'} = K_\tau (E - E') \quad (32)$$

given by the sine kernel in Eq. (9). Inserting these expressions into Eq. (4) we find at zero temperature

$$\chi(\lambda) = \det \left(1 + (e^{i\lambda} - 1) \mathcal{S}_{\text{sys}}^\dagger P_T \mathcal{K}_\tau P_T \mathcal{S}_{\text{sys}} \right), \quad (33)$$

having used that the scattering matrix \mathcal{S}_{sys} is unitary and $P_T + P_R = 1$. In this expression, the increase of the gate voltage δV_g has dropped out. Moreover, by introducing the matrix

$$\mathcal{Q}_\tau = \mathcal{S}_{\text{sys}}^\dagger P_T \mathcal{K}_\tau P_T \mathcal{S}_{\text{sys}}, \quad (34)$$

we may express the moment generating function as

$$\chi(\lambda) = \det \left(1 + (e^{i\lambda} - 1) \mathcal{Q}_\tau \right). \quad (35)$$

Finally, by taking the limit $\lambda \rightarrow i\infty$, we recover the determinant formula for the idle time probability

$$\Pi(\tau) = \det \left(1 - \mathcal{Q}_\tau \right) \quad (36)$$

previously derived in Refs. 7, 17, and 18 without a detector. For a static scatterer with an applied voltage V , the matrix \mathcal{Q}_τ only has non-zero elements in the transport window $[E_F, E_F + eV]$ above the Fermi level.^{17,18}

Next, we consider the non-ideal situation where electrons may complete several loops inside the capacitor and interact with the spin more than once. This is described by the scattering matrix in Eq. (28). We then evaluate the idle time probability by inserting this scattering matrix into Eq. (4). In contrast to Eq. (33), the function $\chi(\lambda)$ now contains terms that are proportional to $\exp(i\lambda/2)$ as shown in App. A. Consequently, the function is not 2π -periodic in λ as required for a moment generating function according to Eq. (16), and it does not correspond to a series of discrete detection events. This may be related to the occurrence of negative probabilities in FCS due to interference effects.⁵¹ Still, we can take the limit $\lambda \rightarrow i\infty$ and calculate the resulting WTD using Eq. (13). However, as we will see, the WTD may then become negative for certain waiting times. This is due to processes where an electron interacts more than once with the spin and thereby tampers with the measurement of the idle time probability.

V. APPLICATIONS

We are now ready to illustrate the electron waiting time clock with two specific applications: A voltage-biased QPC and lorentzian voltage pulses. We also investigate the influence of a smooth transmission profile. In

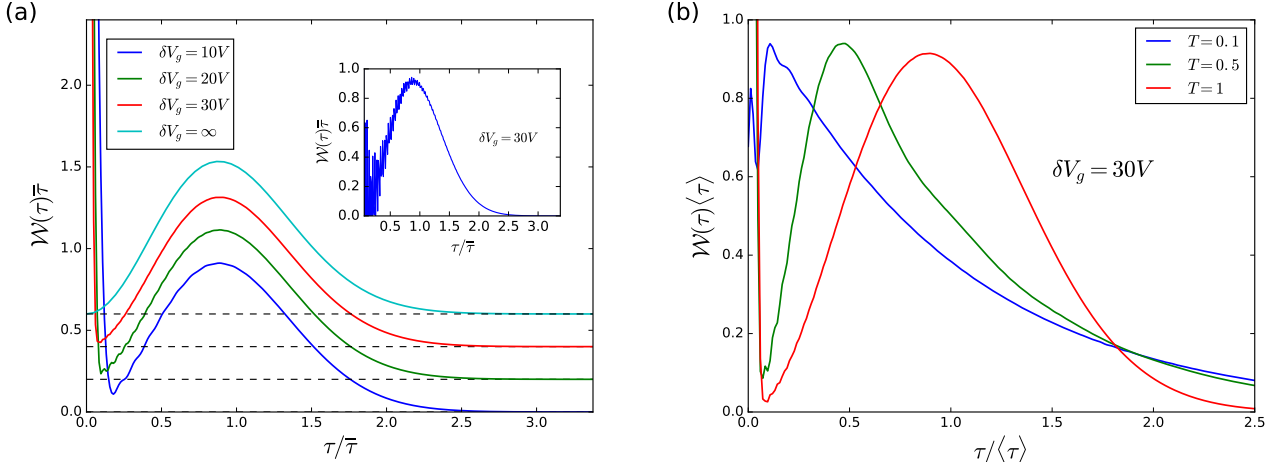


Figure 2. WTDs for a voltage-biased QPC. (a) Distribution of waiting times for a fully transmitting QPC ($T = 1$) with an applied voltage V . The mean waiting time is $\bar{\tau} = h/(eV)$. We show results for different values of the gate voltage increase δV_g . With $\delta V_g = 30V$, we essentially recover the prediction ($\delta V_g = \infty$) of earlier theories without a detector.^{17,18} The curves have been shifted vertically for the sake of a better visibility. We have applied a low pass filter to remove high-frequency oscillations. The inset shows the WTD for $\delta V_g = 30V$ without the low pass filter. (b) Distribution of waiting times for different values of the QPC transmission T . We find a crossover from Wigner-Dyson distribution at full transmission ($T = 1$) to Poisson statistics close to pinch-off ($T = 0.1$) in agreement with earlier work without a detector.^{17,18}

App. B we consider a smooth coupling to the spin instead of the abrupt switching given by Eq. (6). Technically, it is worth mentioning that the Fredholm determinants that appear for example in Eq. (4) can be evaluated efficiently using the algorithm described in Ref. 52.

A. Voltage-biased QPC

We start by considering a QPC with transmission probability T and applied voltage V . In this case, we have $S_{\text{sys}} = \sqrt{T}$. Earlier works^{17,18} without a detector have shown that the WTD should display a cross-over from Wigner-Dyson statistics at full transmission ($T = 1$) to a Poisson distribution close to pinch-off ($T \simeq 0$) with the mean waiting time given as

$$\langle \tau \rangle = \frac{\bar{\tau}}{T}, \quad (37)$$

where

$$\bar{\tau} = \frac{h}{eV}, \quad (38)$$

is the meaning waiting time at full transmission.

Figure 2 shows WTDs obtained with the waiting time clock. We calculate the idle probability using Eqs. (4,28), see also App. A, and differentiate it twice with respect to τ according to Eq. (13). In panel (a) we show the WTD for a fully open QPC with different increments of the gate voltage δV_g . To measure the WTD, the coupling to the spin is only non-zero during a period of time on the order of $\bar{\tau}$. Such short detector pulses can change the energy

of an electron by an amount on the order of $h/\bar{\tau} = eV$. Thus, to ensure that no electrons are scattered below the Fermi level during the measurement, the increase of the gate voltage must be much larger than this energy scale, i. e. $\delta V_g \gg V$. This physical picture is confirmed by panel (a). As we increase δV_g , we approach the results of an ideal clock obtained from Eq. (36).

The time resolution of the waiting time clock depends on δV_g . A finite value of δV_g introduces fluctuations in the WTD on the time scale $h/(e\delta V_g)$. The fluctuations essentially disappear for waiting times that are longer than the mean waiting time, where the measurement-induced disturbances are almost negligible. By contrast, for very short waiting times, the WTD may become negative as seen in the results with $\delta V_g = 10V$. To remove any spurious fluctuations, we apply a low pass filter that suppresses frequencies on the order of $e\delta V_g/h$. The inset of panel (a) shows the WTD without the low pass filter.

In panel (b) we consider the WTD for different values of the QPC transmission T . The figure illustrates how our electron waiting time clock allows a observation of the cross-over from Wigner-Dyson distribution at full transmission to Poisson statistics close to pinch-off as previously predicted by theories without a detector.^{17,18}

B. Lorentzian voltage pulses

Next, we consider lorentzian voltage pulses applied to the input lead.^{3,4,31,53-55} The applied voltage has the

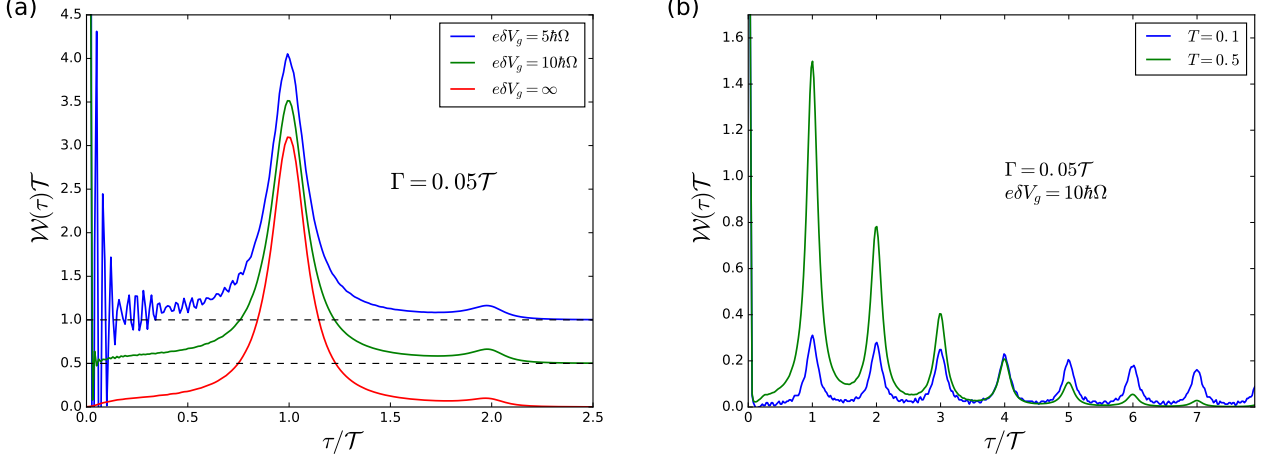


Figure 3. WTDs for levitons transmitted through a QPC. (a) Results for full transmission ($T = 1$) with different values of the gate voltage increase δV_g . Already with $e\delta V_g = 10\hbar\Omega$, the waiting time clock reproduces results ($\delta V_g = \infty$) of earlier theories without a detector.^{7,8} The curves have been shifted vertically for the sake of a better visibility. (b) Results for a QPC with a finite transmission T . In this case, levitons may reflect back on the QPC, and the WTD has peaks at multiples of the period.

form

$$V(t) = \sum_{j=-\infty}^{\infty} \frac{2\hbar\Gamma}{(t - j\mathcal{T})^2 + \Gamma^2}, \quad (39)$$

where Γ denotes the pulse width and \mathcal{T} is the period. The voltage can be encoded in a time-dependent scattering phase picked up by electrons as they leave the lead

$$e^{i\phi(t)} = e^{-i\frac{e}{\hbar} \int_{-\infty}^t V(t') dt'} \quad (40)$$

By Fourier transforming this scattering phase, we obtain a Floquet scattering matrix with elements^{7,56}

$$\mathcal{S}_F(E_n, E) = \begin{cases} -2e^{-n\Omega\Gamma} \sinh(\Omega\Gamma) & \text{if } n > 0 \\ e^{-\Omega\Gamma} & \text{if } n = 0 \\ 0 & \text{otherwise} \end{cases}, \quad (41)$$

where $\Omega = 2\pi/\mathcal{T}$ and $E_n = E + n\hbar\Omega$ with n being an integer. For a periodic voltage, electrons can in general emit or absorb energy quanta of size $\hbar\Omega$. However, for lorentzian pulses (and only in this case), electrons can only absorb energy. Moreover, each pulse excites just a single electron out of the Fermi sea without creating any additional electron-hole pairs. These single-electron excitations are known as levitons.^{3,4} The corresponding scattering matrix reads⁵⁷

$$[\mathcal{S}_{\text{sys}}]_{E, E'} = \sqrt{T} \sum_n \delta(E' - E_n) \mathcal{S}_F(E, E'), \quad (42)$$

having included a QPC that reflects a fraction $R = 1 - T$ of the levitons before they reach the waiting time clock.

Figure 3 shows the distribution of waiting times between levitons measured with the waiting time clock. For a fully transmitting QPC, the WTD is peaked around the

period of the driving \mathcal{T} , panel (a). Unlike the results for the voltage-biased QPC, there is no need to apply a low pass filter. We still observe small oscillations with a period of $h/e\delta V_g$, but they essentially disappear already for $\delta V_g = 10\hbar\Omega/e$. Physically, the levitons are well-localized in time and space, and one would expect that they are easier to distinguish from the underlying Fermi sea than electrons emitted from a constant voltage source. This is indeed confirmed by our results.

In panel (b) we consider the WTD of levitons transmitted through a partially reflecting QPC. In this case, levitons may reflect back on the QPC. As a consequence, the WTD develops peaks at multiples of the period, with each peak corresponding to the number of subsequent reflections that have occurred. Again, we find good agreement with earlier theories without a detector.^{7,8}

C. Smooth QPC transmission

So far, we have considered a waiting time clock with a sharp cut-off in the transmission. In reality, however, the cut-off might be smooth, corresponding to having a finite value of \mathcal{B} in Eq. (20). In this case, electrons below the Fermi level can enter and leave the capacitor, and electrons above the Fermi level may reflect back on the QPC and never enter the capacitor. Figure 4 shows the WTD for a constant voltage V with different values of the cut-off parameter \mathcal{B} . For values of \mathcal{B} that are much larger than the inverse voltage, the influence on the WTD is small compared to the ideal case with a sharp cut-off. For smaller values of \mathcal{B} , the shape of the distribution gets somewhat distorted. Still, a measurement of the WTD is clearly possible with a smooth QPC transmission.

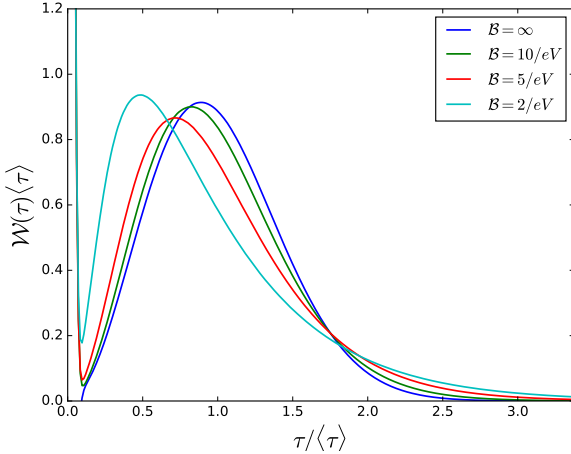


Figure 4. WTDs obtained with a smooth transmission profile. The sharpness of the transmission in Eq. (20) is determined by the parameter \mathcal{B} . We consider here the WTD for a single edge channel with an applied voltage V and have used $\delta V_g = 30V$.

VI. MEASUREMENT SCHEME

The electron waiting time clock relies on measuring the moment generating function $\chi(\lambda, \tau)$ for different values of the counting field λ to obtain the idle time probability via the Fourier transformation in Eq. (17). To this end, it should be possible not only to turn the coupling on and off, but also to accurately change the strength of the coupling as well as measure the off-diagonal element of the spin density matrix. In principle, this is possible. However, as we will show now, a better strategy might be to couple several spins to the mesoscopic capacitor.

We start by considering just a single spin coupled to the capacitor during the time τ . The coupling strength is denoted as λ_1 . The spin is initialized in the pure state

$$|\Psi\rangle = \frac{1}{\sqrt{2}}(|\uparrow\rangle + |\downarrow\rangle) \quad (43)$$

with the corresponding density matrix

$$\hat{\rho}_0^{(1)} = |\Psi\rangle\langle\Psi| = \frac{1}{2} \begin{pmatrix} 1 & 1 \\ 1 & 1 \end{pmatrix}. \quad (44)$$

After the coupling is turned off, the density matrix reads

$$\hat{\rho}^{(1)} = \frac{1}{2} \begin{pmatrix} 1 & \chi^*(\lambda_1, \tau) \\ \chi(\lambda_1, \tau) & 1 \end{pmatrix}. \quad (45)$$

Since the coupling is fixed we cannot extract the moment generating function. However, we can calculate the probabilities of the individual precession angles of the spin. In particular, the probability that the spin is in its initial state after the coupling has been switched off reads

$$\Pi^{(1)}(\tau) = \text{tr}[\hat{\rho}_0^{(1)} \hat{\rho}^{(1)}] = \frac{1}{2} [1 + \text{Re} \chi(\lambda_1, \tau)]. \quad (46)$$

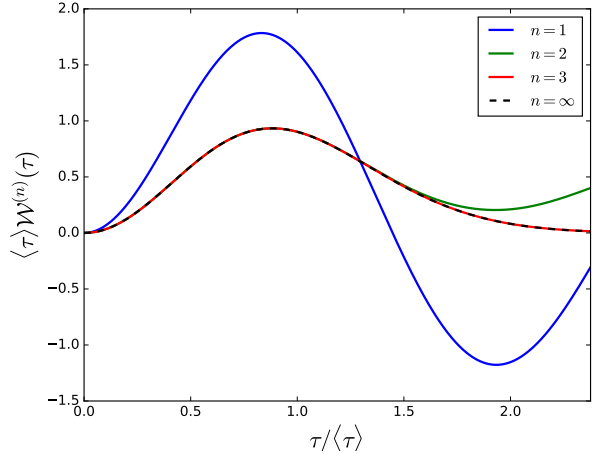


Figure 5. WTDs obtained with n spins coupled to the capacitor. We consider here the WTD for a single edge channel with an applied voltage V and have used $\delta V_g \gg V$. The WTD obtained with a perfect detector is shown with a dashed line.

For $\lambda_1 = \pi$, this is a crude approximation of the integral in Eq. (17). To improve the approximation, we couple a second spin to the capacitor. The coupling strength of this spin is denoted as λ_2 . Both spins are initially in the state given by Eq. (43). If the couplings have been switched on during a time interval of length τ , the elements of the density matrix of the spins become

$$[\hat{\rho}^{(2)}]_{ij,kl} = \frac{1}{4} \chi^{(2)}((i-j)\lambda_1, (k-l)\lambda_2, \tau). \quad (47)$$

Here, the indices $i, j = 0, 1$ (k, l) refer to the first (second) spin and $\chi^{(2)}(\lambda_1, \lambda_2, \tau)$ is a joint moment generating function obtained from Eq. (3) by including the additional scattering phases due to the second spin. If the two spins are directly attached to the capacitor one after another, we find that the joint moment generating function can be expressed as

$$\chi^{(2)}(\lambda_1, \lambda_2, \tau) = \chi(\lambda_1 + \lambda_2, \tau) \quad (48)$$

in terms of the moment generating function $\chi(\lambda, \tau)$ corresponding to a single spin. Calculating the probability that the spins are in their initial states after the couplings have been switched off, we find

$$\Pi^{(2)}(\tau) = \frac{1}{4} [1 + \text{Re} \{\chi(\pi/2, \tau) + \chi(\pi, \tau) + \chi(3\pi/2, \tau)\}], \quad (49)$$

taking $\lambda_1 = \pi/2$ and $\lambda_2 = \pi$. This is now a four-point approximation of the integral in Eq. (17). Following this line of thoughts, one can extend the idea to three or more spins, and thereby further improve the approximation of the idle time probability. For example with 3 spins with couplings $\lambda_1 = \pi/3$, $\lambda_2 = 2\pi/3$, and $\lambda_3 = \pi$, one obtains a six-point approximation of the integral.

In Fig. 5 we show WTDs based on idle time probabilities $\Pi^{(n)}(\tau)$ measured with n ($= 1, 2, 3$) spins. With

just one spin, the WTD is only qualitatively correct for very short waiting times compared with the mean waiting time. At longer times, the WTD turns negative which is clearly not correct. However, already with two spins coupled to the capacitor, the results are much closer to the WTD obtained with a perfect detector. Only for long waiting times, deviations become visible. With three spins coupled to the capacitor, we find essentially perfect agreement with the expected WTD for the range of waiting times shown in Fig. 5.

VII. CONCLUSIONS

We have presented a quantum theory of a waiting time clock which can measure the distribution of waiting times between electrons above the Fermi sea in a mesoscopic conductor. This is an important element which so far has been missing in theories of electron waiting times. Our waiting time clock consists of a mesoscopic capacitor coupled to a quantum two-level system whose coherent precession is measured. We have demonstrated explicitly that the waiting time clock under ideal operating conditions recovers the predictions of earlier theories without a detector. We have also investigated the influence of imperfect operating conditions with two specific applications. With these advances, theories of electron waiting times can now be discussed based on a specific detector.

Our work leaves a number of questions for future investigations. The waiting time clock presented here may not be the only one that can measure the distribution of waiting times between electrons above the Fermi sea. It would be interesting to devise alternative implementations of such waiting time clocks. It might also be interesting to investigate waiting time clocks that are sensitive to the electrons below the Fermi level. The distribution of electron waiting times between electrons in the Fermi sea constitutes a line of research which has not yet been addressed. Finally, the ideas presented here may form the basis for future investigations of the influence of interactions on the distribution of electron waiting times.

ACKNOWLEDGMENTS

We thank W. Belzig, P. P. Hofer, G. B. Lesovik, and E. V. Sukhorukov for stimulating discussions. We acknowledge the computational resources provided by the Aalto Science-IT project and by the Baobab cluster at University of Geneva. D. D. gratefully acknowledges the hospitality of Aalto University. The work was supported by Swiss NSF and Academy of Finland.

Appendix A: Full scattering matrix

If electrons can complete several loops inside the capacitor, the moment generating function reads

$$\begin{aligned} \chi(\lambda, \tau) = \det & \left(\mathcal{S}_{\text{sys}}^\dagger \left(P_R + P_T \mathcal{S}_{-\lambda}^{(l)\dagger} P_T + P_T \mathcal{M}_{-\lambda}^\dagger P_T \right) \right. \\ & \times \left. \left(P_R + P_T \mathcal{S}_\lambda^{(l)} P_T + P_T \mathcal{M}_\lambda P_T \right) \mathcal{S}_{\text{sys}} \right), \end{aligned} \quad (\text{A1})$$

having introduced the matrix

$$\mathcal{M}_\lambda = \mathcal{S}_\lambda^{(l)} P_R \left(1 - P_R \mathcal{S}_\lambda^{(l)} P_R \right)^{-1} P_R \mathcal{S}_\lambda^{(l)} \quad (\text{A2})$$

which describes processes where electrons complete more than one loop. By further manipulations, the moment generating function can be brought on the form

$$\begin{aligned} \chi(\lambda, \tau) = \det & \left(1 + \mathcal{S}_{\text{sys}}^\dagger P_T \left[(\mathcal{K}_\tau^\dagger + \mathcal{K}_\tau) \left(e^{i\lambda/2} - 1 \right) \right. \right. \\ & \left. \left. + \mathcal{K}_\tau^\dagger P_T \mathcal{K}_\tau \left(e^{i\lambda/2} - 1 \right)^2 + \mathcal{R}_\tau^\lambda \right] P_T \mathcal{S}_{\text{sys}} \right) \end{aligned} \quad (\text{A3})$$

with

$$\begin{aligned} \mathcal{R}_\tau^\lambda = & \mathcal{M}_{-\lambda}^\dagger P_T \mathcal{M}_\lambda + \left(\mathcal{L}^\dagger \mathcal{M}_\lambda + \mathcal{M}_{-\lambda}^\dagger \mathcal{L} \right) \\ & + \mathcal{L}^\dagger \mathcal{K}_\tau^{-\lambda\dagger} P_T \mathcal{M}_\lambda + \mathcal{M}_{-\lambda}^\dagger P_T \mathcal{K}_\tau^\lambda \mathcal{L}, \end{aligned} \quad (\text{A4})$$

where the matrix elements of \mathcal{L} read

$$[\mathcal{L}]_{E, E'} = e^{i(E' + e\delta V_g)\tau_D} \delta(E - E' - e\delta V_g). \quad (\text{A5})$$

In this case, the function in Eq. (A3) contains terms that are proportional to $\exp(i\lambda/2)$. This is due to the commutator $[P_T, \mathcal{K}_\tau]$ being non-zero.

Appendix B: Lorentzian switching

As an interesting aside, we consider a smooth coupling to the spin. Specifically, we take $\lambda(t)$ to be the integral of a lorentzian,

$$\lambda(t) = \int_{-\infty}^t \frac{-2\tau}{t'^2 + \tau^2/4} dt' = -2\pi - 4 \arctan(2t/\tau), \quad (\text{B1})$$

such that

$$[U_\tau^{\text{lor}}]_{t, t'} = e^{i\lambda(t)/2} \delta(t - t') = \frac{t + i\tau/2}{t - i\tau/2} \delta(t - t'). \quad (\text{B2})$$

It should be noted that $\lambda(t) \simeq 0$ for $t < -\tau/2$ and $\lambda(t) \simeq -4\pi$ for $t > \tau/2$. However, due to the 4π -periodicity in Eq. (B2), the value $\lambda = -4\pi$ is equivalent to $\lambda = 0$. Thus, one may think of the coupling in Eq. (B1) as being non-zero only during the time interval $[-\tau/2, \tau/2]$.

In the energy representation, the elements of U_τ^{lor} are

$$[U_\tau^{\text{lor}}]_{E, E'} = \delta(E - E') - K_\tau^{\text{lor}}(E - E'), \quad (\text{B3})$$

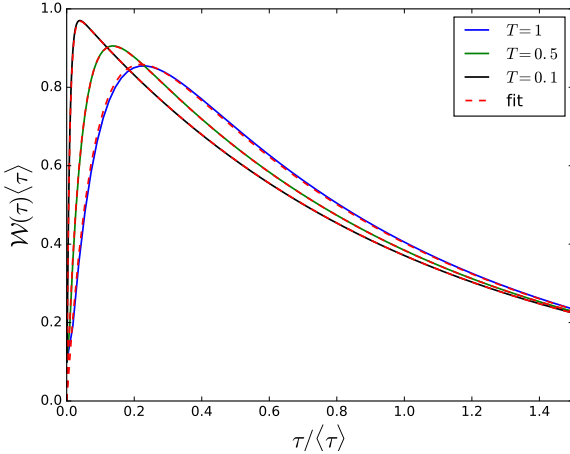


Figure 6. WTDs with a lorentzian switching of the coupling. We show results for a QPC with different transmission probabilities T . The dashed curves are based on Eqs. (B8, B9).

where we have defined the exponential kernel

$$K_\tau^{\text{lor}}(E) = \tau e^{-\tau E/2} \Theta(E). \quad (\text{B4})$$

Unlike the sine kernel in Eq. (9), this kernel is only non-zero for positive energies. Thus, electrons can only absorb energy by interacting with the spin and are thus not scattered into the Fermi sea.

Next, we evaluate Eq. (4) and find

$$\chi(\lambda) = \det(1 - Q_\tau^{\text{lor}}) \quad (\text{B5})$$

with

$$Q_\tau^{\text{lor}} = \mathcal{S}_{\text{sys}}^\dagger P_T K_\tau^{\text{lor}} P_T \mathcal{S}_{\text{sys}} \quad (\text{B6})$$

and

$$[K_\tau^{\text{lor}}]_{E, E'} = \tau e^{-|E - E'| \tau / 2}. \quad (\text{B7})$$

Surprisingly, by comparing these expressions with Eqs. (34,36), we see that Eq. (B5) takes the form of an idle time probability, however, with the kernel given by Eq. (B7). Thus, without further justification, we consider in the following $\chi(\lambda)$ as the idle time probability and evaluate the corresponding WTD by differentiating it twice with respect to τ .

In Fig. 6 we show WTDs for a QPC with transmission T obtained in this way. The mean waiting time is still given by Eq. (37), however, the WTDs are different from those in Fig. 2b. The WTD appears to depend linearly on τ at short times and eventually decays exponentially at long times. This resembles the WTD for a resonant level in the high-bias limit⁵

$$W(\tau) = \frac{\Gamma_L \Gamma_R}{\Gamma_R - \Gamma_L} (e^{-\Gamma_L \tau} - e^{-\Gamma_R \tau}), \quad (\text{B8})$$

where Γ_L and Γ_R are the rates at which electrons enter and leave the level. The mean waiting time reads

$$\langle \tau \rangle = \frac{\Gamma_L + \Gamma_R}{\Gamma_L \Gamma_R}. \quad (\text{B9})$$

Based on the similarity, we surmise that Eq. (B8) also describes the WTDs in Fig. 6. The rate Γ_R can be determined from the mean waiting time. We then use Γ_L to fit our results for full transmission and find excellent agreement. For the results with finite transmission, we keep Γ_L fixed and extract Γ_R from the mean waiting time which depends on the transmission. With this approach, we can fully account for all results in Fig. 6. Further investigations of these findings are left for future work.

¹ E. Bocquillon, V. Freulon, F. D. Parmentier, J.-M. Berroir, B. Plaçais, C. Wahl, J. Rech, T. Jonckheere, T. Martin, C. Grenier, D. Ferraro, P. Degiovanni, and G. Fèvre, “Electron quantum optics in ballistic chiral conductors,” *Ann. Phys.* **526**, 1 (2014).

² G. Fèvre, A. Mahé, J.-M. Berroir, T. Kontos, B. Plaçais, D. C. Glattli, A. Cavanna, B. Etienne, and Y. Jin, “An On-Demand Coherent Single-Electron Source,” *Science* **316**, 1169 (2007).

³ J. Dubois, T. Jullien, F. Portier, P. Roche, A. Cavanna, Y. Jin, W. Wegscheider, P. Roulleau, and D. C. Glattli, “Minimal-excitation states for electron quantum optics using levitons,” *Nature* **502**, 659 (2013).

⁴ T. Jullien, P. Roulleau, B. Roche, A. Cavanna, Y. Jin, and D. C. Glattli, “Quantum tomography of an electron,” *Nature* **514**, 603 (2014).

⁵ T. Brandes, “Waiting times and noise in single particle transport,” *Ann. Phys.* **17**, 477 (2008).

⁶ M. Albert, C. Flindt, and M. Büttiker, “Distributions of Waiting Times of Dynamic Single-Electron Emitters,” *Phys. Rev. Lett.* **107**, 086805 (2011).

⁷ D. Dasenbrook, C. Flindt, and M. Büttiker, “Floquet Theory of Electron Waiting Times in Quantum-Coherent Conductors,” *Phys. Rev. Lett.* **112**, 146801 (2014).

⁸ M. Albert and P. Devillard, “Waiting time distribution for trains of quantized electron pulses,” *Phys. Rev. B* **90**, 035431 (2014).

⁹ D. Dasenbrook, P. P. Hofer, and C. Flindt, “Electron waiting times in coherent conductors are correlated,” *Phys. Rev. B* **91**, 195420 (2015).

¹⁰ P. P. Hofer, D. Dasenbrook, and C. Flindt, “Electron waiting times for the mesoscopic capacitor,” *Physica E* (2016), 10.1016/j.physe.2015.08.034.

¹¹ S. Welack, S. Mukamel, and Y. Yan, “Waiting time distributions of electron transfers through quantum dot Aharonov-Bohm interferometers,” *Europhys. Lett.* **85**, 57008 (2009).

¹² S. Welack and Y. Yan, “Non-markovian theory for the waiting time distributions of single electron transfers,” *J. Chem. Phys.* **131**, 114111 (2009).

¹³ K. H. Thomas and C. Flindt, “Electron waiting times in non-markovian quantum transport,” *Phys. Rev. B* **87**, 121405 (2013).

¹⁴ B. Sothmann, “Electronic waiting-time distribution of a quantum-dot spin valve,” *Phys. Rev. B* **90**, 155315 (2014).

¹⁵ V. Talbo, J. Mateos, S. Retailleau, P. Dollfus, and T. González, “Time-dependent shot noise in multi-level quantum dot-based single-electron devices,” *Semicond. Sci. Technol.* **30**, 055002 (2015).

¹⁶ T. Brandes and C. Emery, “Feedback control of waiting times,” arXiv:1602.02975.

¹⁷ M. Albert, G. Haack, C. Flindt, and M. Büttiker, “Electron Waiting Times in Mesoscopic Conductors,” *Phys. Rev. Lett.* **108**, 186806 (2012).

¹⁸ G. Haack, M. Albert, and C. Flindt, “Distributions of electron waiting times in quantum-coherent conductors,” *Phys. Rev. B* **90**, 205429 (2014).

¹⁹ K. H. Thomas and C. Flindt, “Waiting time distributions of noninteracting fermions on a tight-binding chain,” *Phys. Rev. B* **89**, 245420 (2014).

²⁰ G.-M. Tang, F. Xu, and J. Wang, “Waiting time distribution of quantum electronic transport in the transient regime,” *Phys. Rev. B* **89**, 205310 (2014).

²¹ R. Seoane Souto, R. Avriller, R. C. Monreal, A. Martín-Rodero, and A. Levy Yeyati, “Transient dynamics and waiting time distribution of molecular junctions in the polaronic regime,” *Phys. Rev. B* **92**, 125435 (2015).

²² L. Rajabi, C. Pöltl, and M. Governale, “Waiting Time Distributions for the Transport through a Quantum-Dot Tunnel Coupled to One Normal and One Superconducting Lead,” *Phys. Rev. Lett.* **111**, 067002 (2013).

²³ S. Dambach, B. Kubala, V. Gramich, and J. Ankerhold, “Time-resolved statistics of nonclassical light in Josephson photonics,” *Phys. Rev. B* **92**, 054508 (2015).

²⁴ M. Albert, D. Chevallier, and P. Devillard, “Waiting times of entangled electrons in normal-superconducting junctions,” *Physica E* **76**, 209 (2016).

²⁵ T. Fujisawa, T. Hayashi, R. Tomita, and Y. Hirayama, “Bidirectional Counting of Single Electrons,” *Science* **312**, 1634 (2006).

²⁶ S. Gustavsson, R. Leturcq, B. Simovic, R. Schleser, T. Ihn, P. Studerus, K. Ensslin, D. C. Driscoll, and A. C. Gossard, “Counting Statistics of Single-Electron Transport in a Quantum Dot,” *Phys. Rev. Lett.* **96**, 076605 (2006).

²⁷ S. Gustavsson, R. Leturcq, M. Studer, I. Shorubalko, T. Ihn, K. Ensslin, D. C. Driscoll, and A. C. Gossard, “Electron counting in quantum dots,” *Surf. Sci. Rep.* **64**, 191 (2009).

²⁸ C. Flindt, C. Fricke, F. Hohls, T. Novotný, K. Netočný, T. Brandes, and R. J. Haug, “Universal oscillations in counting statistics,” *Proc. Natl. Acad. Sci. USA* **106**, 10116 (2009).

²⁹ N. Ubbelohde, C. Fricke, C. Flindt, F. Hohls, and R. J. Haug, “Measurement of finite-frequency current statistics in a single-electron transistor,” *Nat. Commun.* **3**, 612 (2012).

³⁰ V. F. Maisi, D. Kambly, C. Flindt, and J. P. Pekola, “Full Counting Statistics of Andreev Tunneling,” *Phys. Rev. Lett.* **112**, 036801 (2014).

³¹ L. S. Levitov, H. Lee, and G. B. Lesovik, “Electron counting statistics and coherent states of electric current,” *J. Math. Phys.* **37**, 4845 (1996).

³² M. Büttiker, “Scattering Theory of Thermal and Excess Noise in Open Conductors,” *Phys. Rev. Lett.* **65**, 2901 (1990).

³³ Ya. M. Blanter and M. Büttiker, “Shot noise in mesoscopic conductors,” *Phys. Rep.* **336**, 1 (2000).

³⁴ U. Gavish, Y. Levinson, and Y. Imry, “Shot-Noise in Transport and Beam Experiments,” *Phys. Rev. Lett.* **87**, 216807 (2001).

³⁵ S. Saito, J. Endo, T. Kodama, A. Tonomura, A. Fukuhara, and K. Ohbayashi, “Electron counting theory,” *Phys. Lett. A* **162**, 442 (1992).

³⁶ B. A. Muzykantskii and Y. Adamov, “Scattering approach to counting statistics in quantum pumps,” *Phys. Rev. B* **68**, 155304 (2003).

³⁷ K. Schönhammer, “Full counting statistics for noninteracting fermions: Exact results and the Levitov-Lesovik formula,” *Phys. Rev. B* **75**, 205329 (2007).

³⁸ W. Belzig and Yu. V. Nazarov, “Full Counting Statistics of Electron Transfer between Superconductors,” *Phys. Rev. Lett.* **87**, 197006 (2001).

³⁹ Yu. V. Nazarov and M. Kindermann, “Full counting statistics of a general quantum mechanical variable,” *Eur. Phys. J. B* **35**, 413 (2003).

⁴⁰ V. Beaud, G. M. Graf, A. V. Lebedev, and G. B. Lesovik, “Statistics of Charge Transport and Modified Time Ordering,” *J. Stat. Phys.* **153**, 177 (2013).

⁴¹ A. Kamenev, *Field Theory of Non-Equilibrium Systems* (Cambridge University Press, 2011).

⁴² A. Shelankov and J. Rammer, “Charge transfer counting statistics revisited,” *Europhys. Lett.* **63**, 485 (2003).

⁴³ F. Hassler, M. V. Suslov, G. M. Graf, M. V. Lebedev, G. B. Lesovik, and G. Blatter, “Wave-packet formalism of full counting statistics,” *Phys. Rev. B* **78**, 165330 (2008).

⁴⁴ A. G. Abanov and D. A. Ivanov, “Allowed Charge Transfers between Coherent Conductors Driven by a Time-Dependent Scatterer,” *Phys. Rev. Lett.* **100**, 086602 (2008).

⁴⁵ A. G. Abanov and D. A. Ivanov, “Factorization of quantum charge transport for noninteracting fermions,” *Phys. Rev. B* **79**, 205315 (2009).

⁴⁶ R. Vyas and S. Singh, “Waiting-time distributions in the photodetection of squeezed light,” *Phys. Rev. A* **38**, 2423 (1988).

⁴⁷ H. J. Carmichael, S. Singh, R. Vyas, and P. R. Rice, “Photoelectron waiting times and atomic state reduction in resonance fluorescence,” *Phys. Rev. A* **39**, 1200 (1989).

⁴⁸ M. Büttiker, H. Thomas, and A. Prêtre, “Mesoscopic capacitors,” *Phys. Lett. A* **180**, 364 (1993).

⁴⁹ A. Prêtre, H. Thomas, and M. Büttiker, “Dynamic admittance of mesoscopic conductors: Discrete-potential model,” *Phys. Rev. B* **54**, 8130 (1996).

⁵⁰ M. Büttiker, “Quantized transmission of a saddle-point constriction,” *Phys. Rev. B* **41**, 7906 (1990).

⁵¹ P. P. Hofer and A. A. Clerk, “Negative Full Counting Statistics Arise from Interference Effects,” *Phys. Rev. Lett.* **116**, 013603 (2016).

⁵² F. Bornemann, “On the numerical evaluation of Fredholm determinants,” *Math. Comp.* **79**, 871 (2010).

⁵³ J. Keeling, I. Klich, and L. S. Levitov, “Minimal Excitation States of Electrons in One-Dimensional Wires,” *Phys. Rev. Lett.* **97**, 116403 (2006).

⁵⁴ D. A. Ivanov, H. W. Lee, and L. S. Levitov, “Coherent states of alternating current,” *Phys. Rev. B* **56**, 6839 (1997).

⁵⁵ A. V. Lebedev, G. B. Lesovik, and G. Blatter, “Generating spin-entangled electron pairs in normal conductors using

voltage pulses,” *Phys. Rev. B* **72**, 245314 (2005).

⁵⁶ J. Dubois, T. Jullien, C. Grenier, P. Degiovanni, P. Roulleau, and D. C. Glattli, “Integer and fractional charge Lorentzian voltage pulses analyzed in the framework of photon-assisted shot noise,” *Phys. Rev. B* **88**, 085301 (2013).

⁵⁷ M. V. Moskalets, *Scattering Matrix Approach to Non-Stationary Quantum Transport* (Imperial College Press, 2011).